ChemComm

COMMUNICATION

View Article Online
View Journal

Cite this: DOI: 10.1039/c8cc09285k

Received 22nd November 2018,
Accepted 11th January 2019

DOI: 10.1039/c8cc09285k

rsc.li/chemcomm

Synergistic catalysis for light-driven proton reduction using a polyoxometalate-based Cu–Ni heterometallic–organic framework†

Wenlong Sun,[a] Cheng He,[a] Tao Liu[a] and Chunying Duan *[ab]

Synergistic effects of bimetallic Ni and Cu supported on metal–organic polymer composites based on Wells–Dawson $P_2W_{18}O_{62}^{6-}$ clusters as photosensitizer units were identified, and we report a novel approach for addressing these issues for dehydrogenation and hydrogen production reactions.

The development of novel and highly efficient materials for dehydrogenation and hydrogen (H_2) production from organic transformations is fundamentally important in the development of oxidative and reductive coupling reactions as well as in potential applications such as hydrogen-storage materials and the conversion of solar energy into hydrogen fuel.[1–10] Transition metal (Ni and Cu) composite materials, which are earth-abundant and relatively inexpensive materials, have been used for the reduction of protons for hydrogen evolution. Bimetallic Ni–Cu materials have been reported to exhibit higher catalytic activity in thermal H_2 evolution than can be achieved with materials composed of Ni or Cu alone.[11–13] These bimetallic Ni–Cu supported materials have also been shown to be effective photocatalysts for reductive hydrogen evolution in the presence of an additional photosensitizer.[11,13] The identification of new cocatalyst-free and self-sensitized polymers for dehydrogenation and hydrogen production without any other additives is of great importance.

A variety of materials have been exploited for these processes.[1–13] Among such species, metal–organic polymers have emerged as an interesting class of porous crystalline materials that can easily possess photosensitizer and metal activating sites that make them catalytically active.[14–17] Polyoxometalates are well known photosensitive materials that have the potential to facilitate multi-electron transfer reactions for light-driven hydrogen evolution.[14] Imbedding POMs into the pores of frameworks has re-emerged as a promising approach to stabilize and heterogenize these redox active catalysts for photocatalytic hydrogen evolution; in most reported examples, noble metal (Ru/Ir)-coordinated pyridine organic derivatives are required as photosensitizers.[15–17]

Considering the above results, we successfully synthesized the first example of a polyoxometalate-based polymer containing bimetallic Ni–Cu ions as the active nodes for oxidative dehydrogenation and reductive hydrogen production. The polymer design included the incorporation of the Wells–Dawson $P_2W_{18}O_{62}^{6-}$ cluster as a photosensitizer unit into the pores of a well-established redox-active mixed-metal copper and nickel organic polymer. We proposed a reaction mechanism for this transformation as shown in Scheme 1. The photocatalytic dehydrogenation and hydrogen evolution that occurs because of the unique photoredox properties of the excited state of the $P_2W_{18}O_{62}^{6-}$ anion enabled the heteropolyacid to catalyse the direct oxidation of the substrates *via* ultraviolet irradiation, and the heteropolyacid formed heteropolyblue. The resulting heteropolyblue could be excited by UV irradiation to reach a new excited state and further reduce the redox-active Cu/Ni sites. The water-coordinated Cu/Ni centres with a suitable redox potential reduce protons for achieving hydrogen evolution, completing the oxidative dehydrogenation and reductive hydrogen production over the entire catalytic cycle.[14]

Single-crystal X-ray diffraction analysis revealed that Cu–Ni–POMs crystallize in the monoclinic space group *P*6/*m*. In our multifunctionalised coordinated polymers, the $[P_2W_{18}O_{62}]^{6-}$

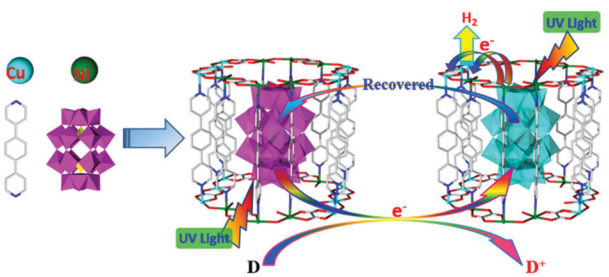

Scheme 1 Diagram illustrating the process of the photocatalytic reaction.

[a] Chemical School of Zhang Dayu State Key Laboratory of Fine Chemicals, Dalian University of Technology, Dalian 116024, China. E-mail: cyduan@dlut.edu.cn
[b] Collaborative Innovation Center of Chemical Science and Engineering, Tianjin 300071, China

† Electronic supplementary information (ESI) available: Experimental details, crystal structure and data for catalytic reactions. CCDC 1875777. For ESI and crystallographic data in CIF or other electronic format see DOI: 10.1039/c8cc09285k

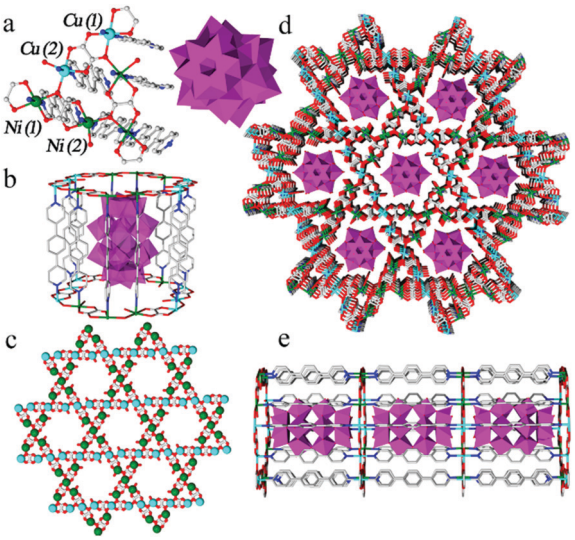

Fig. 1 (a) Diagram of the coordination environment of the $P_2W_{18}O_{62}^{6-}$ cluster, and Cu^{2+} and Ni^{2+} ions. (b) View of a single molecule cage, showing the constituents and fragments, *i.e.*, $P_2W_{18}O_{62}^{6-}$, OX, Cu^{II}, Ni^{II} and PBPY. (c) View of a two-dimensional layer Kagomé structure. (d) View of the front face of a three-dimensional structure showing embedded $P_2W_{18}O_{62}^{6-}$ units within the pores along the *b* axis direction. (e) Side view of a one-dimensional pore structure (nanotube) in (d) formed by the ligands with embedded $[P_2W_{18}O_{62}]^{6-}$ units in the interior.

ions act as photosensitive and photooxidation centres,[14,18] and the Cu–Ni–POM was designed with Cu(II)/Ni(II) as the metal nodes and 4,4′-(1,4-phenylene)bis-pyridine (PBPY) and oxalate (OX) linkers to balance the charge of the $[P_2W_{18}O_{62}]^{6-}$ anions (Fig. 1a). The Cu/Ni ions were coordinated in an octahedral geometry, where Cu(1)/Ni(1) is connected to four oxygen atoms from two OX molecules and two nitrogen donors from two PBPY ligands, and Cu(2)/Ni(2) is coordinated to four oxygen atoms from one water molecule and two OX molecules and two nitrogen donors from two PBPY ligands (Fig. 1a). The unique coordination geometry of the Cu(2)/Ni(2) centres with open axial sites to allow H_2O coordination is the source of the redox activity and proton-activation sites for the electrochemical hydrogen evolution from water.[14]

These two types of Cu/Ni ions are alternately connected *via* corner-sharing oxygen atoms from OX anions to form a two-dimensional sheet with a Kagomé structure (Fig. 1c). The two-dimensional Kagomé structure within the polymers consists of triangular and hexagonal structures (Fig. S2, ESI†). The adjacent sheets are connected by rigid PBPY ligands *via* Cu–N/Ni–N bonds to form three-dimensional cationic pores along the axes (Fig. S3 and S4, ESI†). Along the *b* axis (Fig. 1e), the 1D nanotubes have a diameter of 12.3 Å and can serve as a cage for a single molecule. The tubes are made of the constituents and fragments, *i.e.*, $[P_2W_{18}O_{62}]^{6-}$, OX, Cu^{II}, Ni^{II} and PBPY (Fig. 1b), and each of the isolated voids in the 1D nanotube is occupied by $[P_2W_{18}O_{62}]^{6-}$ anions (Fig. 1d and e) arranged like train cars. The redox-active metal centres and photosensitizing $[P_2W_{18}O_{62}]^{6-}$ centres are sufficiently close in proximity that the potential photoinduced electron transfer from the photosensitizer to the redox-active Cu(2)/Ni(2) centres is efficient and direct, which allows the new polymers to photocatalytically split water into hydrogen; the PLATON program was used to calculate the void volume at approximately 210 Å.^{3} Confocal laser scanning microscopy exhibited strong green fluorescence (λ_{ex} = 520 nm) attributable to the emission of the fluorescein dye (Fig. S6, ESI†), confirming that the uptake of the dye molecules by the crystals of the MOF was unsuccessful. The dye molecules cannot deeply penetrate the internal crystal framework. Furthermore, the results demonstrated that the catalytic process should occur on the surface of the material.

We could obtain Cu–POM and Ni–POM single-crystal structures, but scaling up the syntheses of Cu–POM or Ni–POM was difficult, which is not conducive to industrialization or catalytic experiments. Cu–Ni–POM not only possesses Cu–POM and Ni–POM structural motifs but can also be produced on a large scale, which is beneficial for industrialization and catalytic experiments. ICP-MS analysis of the Cu–Ni–POM showed that it contained equal portions of copper and nickel (1 : 1). The solid-state UV-vis absorption spectra of Zn–POM[14] exhibited a polyoxometalate-based broad absorption band at 200–400 nm, which was assigned to $P_2W_{18}O_{62}^{6-}$ (Fig. S7, ESI†). The solid-state UV-vis absorption spectrum of Cu–Ni–POM exhibited a polyoxometalate-based broad absorption band at 200–400 nm and an additional visible metal (Cu)-to-ligand-to-metal (Ni) charge-transfer band at 500–1000 nm (Fig. S11, ESI†). The spectrum of Cu–Ni–POM showed an emission band at approximately 409 nm (Fig. S9, ESI†). In this case, the free energy change (E^{0-0}) between the ground state and the vibrationally related excited state was approximately 3.10 eV (Fig. S12, ESI†), and this high excitation energy created an active excited state for the photooxidation of substrates or electron donors. Electrochemical measurements of Cu–Ni–POM showed six redox peaks, with four of them attributable to $[P_2W_{18}O_{62}]^{6-}$; the first two redox couples (I and II) correspond to one-electron redox processes that can induce oxidative reactions, and the last two redox couples (III and IV) correspond to two-electron redox processes (Fig. 2a).[14,15] Peaks V and VI correspond to the Cu^{2+} and Ni^{2+} redox peaks (Fig. 2b), respectively. Indeed, the addition of Et_3NH^+ to the Cu–Ni–POM in aqueous media leads to new waves near the redox peaks at approximately −1.5 (VI), −0.95 (V) and −0.7 (IV, V) that increase in intensity with increasing acid concentration (Fig. 2c), indicating that the Cu–Ni–POM acts as an electrocatalyst for proton reduction.[19,20]

The ultraviolet-light-driven catalytic activity of Cu–Ni–POM for hydrogen evolution is given in Table S2 (ESI†). The optimal conditions were found to be a H_2O/Me_2CO (1 : 2 by volume) solution containing Cu–Ni–POM and MeOH (25% v/v). When Zn–POM or $K_6P_2W_{18}O_{62}$ was used as the photocatalyst, little hydrogen evolution was detected under the same experimental conditions (Fig. 3b). A mixture solution of $K_6P_2W_{18}O_{62}$ and $Ni(NO_3)_2$ (TON approximately 210) or $K_6P_2W_{18}O_{62}$ and $Cu(NO_3)_2$ (TON approximately 110) hydrogen gas were generated exhibited a higher turnover number than were generated when using Zn–POM (TON approximately 18) or $K_6P_2W_{18}O_{62}$ (TON approximately 18) as the photocatalyst after irradiation for 65 h (Fig. 3b). These results confirm that copper and nickel are the catalytic sites for the reduction of protons to hydrogen. A mixture of $K_6P_2W_{18}O_{62}$ and

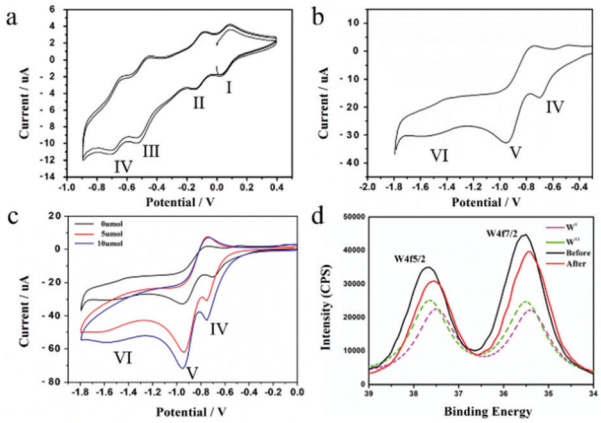

Fig. 2 (a and b) Solid-state cyclic voltammograms of Cu–Ni–POM at a scan rate of 50 mV s^{-1}. (c) Cyclic voltammograms of Cu–Ni–POM containing 0.1 mM $TBAPF_6$ (black line) in the presence of different concentrations of $HNEt_3Cl$ [5 μmol (red line) and 10 μmol (blue line) at a scan rate of 50 mV s^{-1}]. (d) X-ray photoelectron spectroscopy spectra of W 4f in heteropoly before irradiation (black line) and after irradiation (red line).

$Ni(NO_3)_2/Cu(NO_3)_2$ at the same concentration produced only a very low yield of hydrogen compared to the aforementioned mixed copper–nickel-based Cu–Ni–POM system (TON = 550) after irradiation for 65 h (Fig. 3b). This result confirms that hydrogen production is more rapid in a mixed-metal system than in a single metal system. The almost linear increase in the hydrogen evolution with increasing concentration of Cu–Ni–POM in the time dependence curves of hydrogen evolution suggested that the photocatalytic systems were quite stable (Fig. 3a). A catalyst loading of approximately 1 mg produced approximately 1.2 mL of hydrogen gas after irradiation for 65 h (turnover frequency *ca.* 833 μmol g^{-1} h^{-1}), and the calculated turnover number of the entire reaction was approximately 550 per mole of Cu–Ni–POM catalyst (Fig. 3a and b). We compare with the relative studies,[15,17,21] these similar heterogeneous (MOFs) photocatalysis hydrogen evolution reaction relatively low efficiency need the presence of noble metal catalyst, and the similar homogeneous (POMs) photocatalysis reaction need the presence of an additional noble metal photosensitizer. Cu–Ni–POM represents a single catalyst that exhibits a higher activity without any other additives.

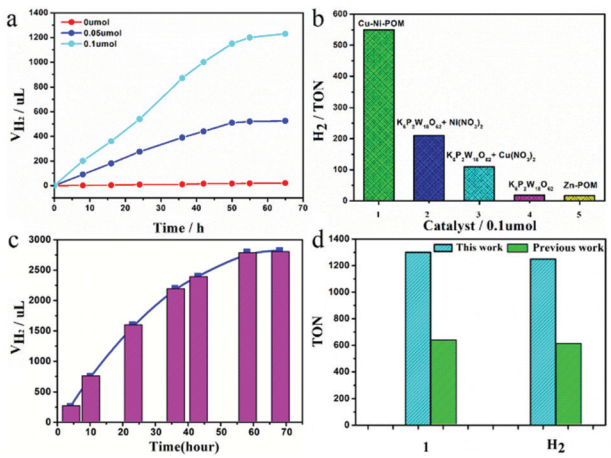

Fig. 3 (a) Volume of evolved hydrogen as a function of time using Cu–Ni–POM (0 μmol, 0.05 μmol or 0.1 μmol based on the molecular cage unit) in a H_2O/Me_2CO (1 : 2 by volume) solution containing MeOH (25% v/v) after light irradiation for 65 h (200–400 nm). (b) Calculated turnover numbers of different catalysts in photoreductive hydrogen production in a H_2O/Me_2CO (1 : 2 by volume) solution containing MeOH (25% v/v) after light irradiation for 65 h (200–400 nm). (c) Volume of evolved hydrogen as a function of time using Cu–Ni–POM (0.1 μmol). (d) Calculated turnover numbers of Cu–Ni–POM (this work) and Co–POM (previous work) in the catalytic dehydrogenation of tetrahydroisoquinoline to produce 3,4-dihydroisoquinoline (**1**) and hydrogen gas in H_2O/Me_2CO (1 : 3 by volume) as the solvent. *V* = 5.5 mL.

The XPS spectrum indicates that after the photocatalytic reaction, the W^{VI} centres in the Cu–Ni–POM anions are converted into W^{V}, forming an excited-state POM species[14] (Fig. 2d). Photocatalysis by Cu–Ni–POM compounds was first characterized by colour changes of the reaction mixtures from colourless to blue suspensions, which is an indication of the reduction of W(VI). The colour remained if the system was exposed to light. However, re-oxidation of W(V) to W(VI) occurred within hours of exposure to air or oxygen with concomitant decolouration of the blue suspension (Fig. S15, ESI†).[14] These experimental results reveal that the excited state POM first receives electrons from the MeOH to form the heteropolyblue species. The latter absorbs photons to reach its excited state and undergoes photoinduced electron transfer to the copper or nickel centres. Coordination of a water molecule to the copper or nickel centres and the formation of low-valence copper or nickel species further reduce protons to generate hydrogen, whereas the excited-state heteropolyblue-POM species are converted back to ground state POM species to complete the overall catalytic cycle.

Heteropolyblue has two absorption bands; the visible absorption band is centred at 650 nm, and the broad ultraviolet absorption band is at 200–350 nm (Fig. S8, ESI†). In this work, we use the heteropolyblue ultraviolet absorption broadband at 200–350 nm with 200–400 nm UV photons to excite the POM to obtain electrons to generate heteropolyblue and ultraviolet photons to excite heteropolyblue (UV absorption band in 200–350 nm) photoinduced electron transfer to reduce the mix-metal Cu and Ni ions to produce hydrogen. In addition, the photocatalytic dehydrogenation of tetrahydroisoquinoline and hydrogen production with Cu–Ni–POM were compared with those of Co–POM (previous work).[14] A solution containing Cu–Ni–POM (1 mg, 0.1 μmol) and tetrahydroisoquinoline (3 mmol) in H_2O/Me_2CO (1 : 3) generated 3,4-dihydroisoquinoline (**1**) (turnover number *ca.* 1300) and hydrogen gas (turnover number *ca.* 1250) using 200–400 nm irradiation for 68 hours (Fig. 3d). A catalyst loading of approximately 1 mg produced 2.8 mL of hydrogen gas after irradiation for 68 h (Fig. 3c). The Cu–Ni–POM (this work) exhibited a higher activity than Co–POM in the catalytic dehydrogenation of tetrahydroisoquinoline and hydrogen production (Fig. 3d). In the Cu–Ni–POM, the Cu, Ni and POM act as electrocatalysts for proton reduction (Fig. 2c), because the catalytic dehydrogenation of tetrahydroisoquinoline and hydrogen production occur more rapidly from the heterometal Cu–Ni ions and POM concerted catalysis centres than with Co–POM alone (previous work). These experiments confirm that the Cu–Ni–POM framework, which allows a concerted mechanism, exhibited higher activity.

Table 1 Reaction of aryl iodides with nitrogen-containing heterocycles[a]

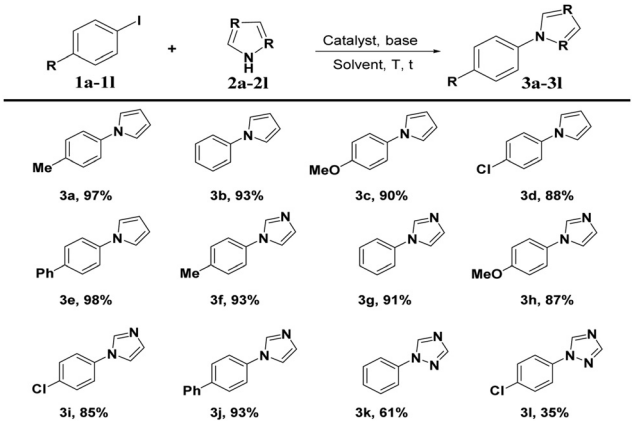

[a] Reaction conditions: **1a–1l** (0.5 mmol), **2a–2l** (1 mmol), catalyst (0.4 mmol% based on the molecule cage unit in Fig. 1b), NaOH (1.0 mmol), DMSO (1 mL), 120 °C, 12 h. Isolated yield.

The C–N bond forming experiments confirm that the concerted reaction with the Cu–Ni–POM catalysis was rapid. The experimental results are listed in Table S1 (ESI†). Either $Cu(NO_3)_2$ (10%) or MOF-199 (2.5%) was used as the catalyst under the same reaction conditions, and they provided obviously lower yields than those achieved with Cu–Ni–POM (0.4%). The results demonstrated that the concerted reactions with the copper metal (catalyst) and nickel metal/POM (cocatalyst) were more efficient. Under the optimal conditions, the scope of the Cu–Ni–POM catalyst system was explored using various aryl iodides and N-containing heterocycles. As shown in Table 1, in general, the N-containing heterocycles with high numbers of nitrogen atoms (1*H*-1,2,4-triazole) gave the coupling products in lower yields (**3k**, **3l**). We proposed that the Cu–Ni–POM active site coordinated to the nitrogen atoms in the nitrogen-dense substrates; therefore, substrates containing fewer nitrogen atoms exhibited higher activities than those with high nitrogen contents (Table 1). The coupling reaction proceeded smoothly for most of the aryl iodides having electron-rich, electron-neutral or electron-deficient groups (but electron-rich and electron-neutral groups were favoured) and afforded the corresponding products in good to excellent yields (**3a**, **3b**, **3e**, **3f**, **3g**, **3j** and **3k**). In general, the electron-deficient substrates gave the coupling products in lower yields (**3c**, **3d**, **3h**, **3i** and **3l**), and the electron-rich indole substrate exhibited a higher activity than the electron-deficient indole substrate (Table 1). To better verify the structure of the catalyst surface, scanning electron microscopy (SEM) measurements were performed. The SEM images of the initial Cu–Ni–POM displayed particle sizes of approximately 0.16–0.19 mm, which showed a catalytic yield of 79% of **3a** after 12 hours. Fine crystalline material with particle sizes of 0.5–2.5 μm, which was prepared by grinding Cu–Ni–POM crystals, displayed a catalytic yield of 97% of **3a** after 12 hours (Fig. S16, ESI†). These results demonstrated that the surface area is a crucial factor in achieving a high yield.

In summary, we have demonstrated a new cocatalyst-free and self-sensitized catalytic system for hydrogen production by exploiting the catalytic activity of bimetallic Cu–Ni supported on metal–organic polymer composites based on the polyoxometalate $P_2W_{18}O_{62}^{6-}$ as a photosensitizer unit. In addition, Cu–Ni–POM bimetallic species are efficient and stable photocatalysts for dehydrogenation and hydrogen evolution under irradiation with UV light. To the best of our knowledge, this is the first work employing a POM material with integrated bimetallic Cu–Ni species to produce H_2 fuel and a valuable organic compound. We believe that this strategy provides promising and practical solutions for converting solar energy into hydrogen fuel and for conducting organic oxidation reactions to generate valuable compounds.

This work was supported by the National Natural Science Foundation of China (No: U1608224 and 21531001).

Conflicts of interest

There are no conflicts to declare.

Notes and references

1 G. E. Dobereiner, A. Nova, N. D. Schley, N. Hazari, S. J. Miller, O. Eisenstein and R. H. Crabtree, *J. Am. Chem. Soc.*, 2011, **133**, 7547.
2 S. Pullen, H. H. Fei, A. Orthaber, S. M. Cohen and S. Ott, *J. Am. Chem. Soc.*, 2013, **135**, 16997.
3 Y. Qin and M. Oestreich, *Angew. Chem., Int. Ed.*, 2017, **56**, 7716.
4 X. Chen, S. Shen, L. Guo and S. S. Mao, *Chem. Rev.*, 2010, **110**, 6503.
5 K. H. He, F. F. Tan, C. Z. Zhou, G. J. Zhou, X. L. Yang and Y. Li, *Angew. Chem., Int. Ed.*, 2017, **56**, 3080.
6 T. Zhang and W. B. Lin, *Chem. Soc. Rev.*, 2014, **43**, 5982.
7 J. Zhang, Y. Chen and X. Wang, *Energy Environ. Sci.*, 2015, **8**, 3092.
8 D. Z. Zee, T. Chantarojsiri, J. R. Long and C. J. Chang, *Acc. Chem. Res.*, 2015, **48**, 2027.
9 F. C. Leng, H. Liu, M. L. Ding, Q. P. Lin and H. L. Jiang, *ACS Catal.*, 2018, **8**, 4583.
10 D. Y. Shi, R. Zheng, M. J. Sun, X. R. Cao, C. X. Sun, C. J. Cui, C. S. Liu, J. W. Zhao and M. Du, *Angew. Chem., Int. Ed.*, 2017, **56**, 14637.
11 Y. Yamada, S. Shikano, T. Akita and S. Fukuzumi, *Catal. Sci. Technol.*, 2015, **5**, 979.
12 Y. W. Zhang, W. Y. Huang, S. E. Habas, J. N. Kuhn, M. E. Grass, Y. Yamada, P. D. Yang and G. A. Somorjai, *J. Phys. Chem. C*, 2008, **112**, 12092.
13 Y. J. Hao, S. Z. Kang, X. Liu, X. Q. Li, L. X. Qin and J. Mu, *ACS Sustainable Chem. Eng.*, 2017, **5**, 1165.
14 W. L. Sun, B. W. An, B. Qi, T. Liu, M. Jin and C. Y. Duan, *ACS Appl. Mater. Interfaces*, 2018, **10**, 13462.
15 Z. M. Zhang, T. Zhang, C. Wang, Z. K. Lin, L. S. Long and W. B. Lin, *J. Am. Chem. Soc.*, 2015, **137**, 3197.
16 X. J. Kong, Z. K. Lin, Z. M. Zhang, T. Zhang and W. B. Lin, *Angew. Chem., Int. Ed.*, 2016, **55**, 6411.
17 J. Tian, Z. Y. Xu, D. W. Zhang, H. Wang, S. H. Xie, D. W. Xu, Y. H. Ren, H. Wang, Y. Liu and Z. T. Li, *Nat. Commun.*, 2016, **7**, 11580.
18 S. S. Wang and G. Y. Yang, *Chem. Rev.*, 2015, **115**, 4893.
19 X. Jing, Y. Yang, C. He, Z. D. Chang, J. N. H. Reek and C. Y. Duan, *Angew. Chem., Int. Ed.*, 2017, **56**, 11759.
20 X. Y. Dong, M. Zhang, R. B. Pei, Q. Wang, D. H. Wei, S. Q. Zang, Y. T. Fan and T. C. W. Mak, *Angew. Chem., Int. Ed.*, 2016, **55**, 2073.
21 H. J. Lv, W. W. Guo, K. F. Wu, Z. Y. Chen, J. Bacsa, D. G. Musaev, Y. V. Geletii, S. M. Lauinger, T. Q. Lian and C. L. Hill, *J. Am. Chem. Soc.*, 2014, **136**, 14015.

